FOAM MICROMECHANICS

Structure and Rheology of Foams, Emulsions, and Cellular Solids

ANDREW M. KRAYNIK
Sandia National Laboratories
Department 9112 MS0834
Albuquerque, New Mexico 87185-0834 USA

MICHAEL K. NEILSEN
Sandia National Laboratories
Department 9117 MS0443
Albuquerque, New Mexico 87185-0443 USA

DOUGLAS A. REINELT
Southern Methodist University
Department of Mathematics
Dallas, Texas 75275-0156 USA

AND

WILLIAM E. WARREN
Texas A&M University
Department of Civil Engineering
College Station, Texas 77843-3136 USA

1. Introduction

Foam evokes many different images: waves breaking at the seashore, the head on a pint of Guinness, an elegant dessert, shaving, the comfortable cushion on which you may be seated... From the mundane to the high tech, foams, emulsions, and cellular solids encompass a broad range of materials and applications. Soap suds, mayonnaise, and foamed polymers provide practical motivation and only hint at the variety of materials at issue.

Typical of multiphase materials, the rheology or mechanical behavior of foams is more complicated than that of the constituent phases alone, which may be gas, liquid, or solid. For example, a soap froth exhibits a static shear modulus–a hallmark of an elastic solid–even though it is composed primarily of two Newtonian fluids (water and air), which have no shear

To appear in the Proceedings of the NATO Advanced Study Institute on "Foams, Emulsions, and Cellular Materials," which was held in Cargese, Corsica, May 11-24, 1997. The proceedings will be edited by Jean-Francois Sadoc and Nicolas Rivier, and published by Kluwer.

DISCLAIMER

modulus. This apparent paradox is easily resolved. Soap froth contains a small amount of surfactant that stabilizes the delicate network of thin liquid films against rupture. The soap-film network deforms in response to a macroscopic strain; this increases interfacial area and the corresponding surface energy, and provides the strain energy of classical elasticity theory [1]. This physical mechanism is easily imagined but very challenging to quantify for a realistic three-dimensional soap froth in view of its complex geometry. Foam micromechanics addresses the connection between constituent properties, cell-level structure, and macroscopic mechanical behavior.

This article is a survey of micromechanics applied to gas-liquid foams, liquid-liquid emulsions, and cellular solids. We will focus on static response where the foam deformation is very slow and rate-dependent phenomena such as viscous flow can be neglected. This includes nonlinear elasticity when deformations are large but reversible. We will also discuss elastic-plastic behavior, which involves yield phenomena.

Foam structures based on polyhedra packed to fill space provide a unifying geometrical theme. Because a two-dimensional situation is always easier to visualize and usually easier to analyze, the roots of foam micromechanics lie in the plane packed with polygons. There are striking similarities as well as obvious differences between 2D and 3D.

Many of the issues investigated here have been reviewed by Weaire & Fortes [2], who also discussed stress and strain in liquid and solid foams. Kraynik [3] has surveyed fluid-fluid systems. Useful reviews on the mechanics of cellular solids include Gibson & Ashby [4] and Kraynik & Warren [5]. The rigorous theoretical foundations and computational details associated with foam micromechanics are beyond the scope of this article. The interested reader is refered to the literature to pursue more technical matters.

2. Theoretical Approach

We only consider spatially periodic models, which are based on a representative volume (unit cell) of foam, countless identical copies of which fit together to fill space. The obvious advantages of spatial periodicity include rigorous mathematical formulation and tractability. The unit cell in the simplest models only contains one foam cell. These *perfectly ordered* models composed of identical cells are most likely to admit analytic solutions, which reveal important physics and can be used to validate computer codes. The unit cell in more complete models will contain many foam cells of different size and shape; a large number of cells N is required to represent the disorder and polydispersity found in real foams.

Spatial periodicity refers to situations where any position-dependent property $\mathcal{P}(\mathbf{x}) = \mathcal{P}(\mathbf{x} + \sum_k i_k \mathbf{L}_k)$, where $\mathbf{x}$ is position, the i_k are arbitrary integers, and the $\mathbf{L}_k$ are lattice vectors. A homogeneous deformation is imposed on the entire foam by applying displacements through the lattice vectors. The local forces or stress $\boldsymbol{\sigma}'(\mathbf{x})$ within the foam are determined by solving balance equations that reflect the appropriate physics. The effective macroscopic stress tensor $\boldsymbol{\sigma}$ is given by the volume average of local stress $\boldsymbol{\sigma}'$ as

$$\boldsymbol{\sigma} = \frac{1}{\mathcal{V}} \int \boldsymbol{\sigma}' dv \tag{1}$$

where $\mathcal{V}$ is the volume of the unit cell. Components of $\boldsymbol{\sigma}$ can also be obtained by using energy methods, which involve derivatives of energy with respect to strain; however, calculations based on (1) frequently offer computational advantages in addition to more information. Force methods, which are based on (1), are especially convenient for evaluating effective stress when the foam is not undergoing macroscopic deformation.

The specific problem to be solved can cross the boundaries of traditional fluid mechanics and solid mechanics, reminding us that foam science and technology, in general, are highly interdisciplinary pursuits involving scientists and engineers from many fields.

3. Two Dimensions

3.1. FOAM STRUCTURE

The structure of gas-liquid foams and liquid-liquid emulsions under static conditions is governed by energy minimization. We neglect gravity so liquid drainage and the resulting spatial inhomogeniety of the foam structure will not be considered. Plateau's laws [6] determine film-network geometry in the limiting case of a *dry* soap froth, which contains negligible liquid. Polyhedral cells in 3D are separated by surfaces (faces) with constant mean curvature (CMC); three curved faces meet at equal dihedral angles of 120° along each edge; and four edges meet at each vertex at equal tetrahedral angles of $\cos^{-1}(-1/3)$=109.47°.

In 2D, Plateau's laws require polygonal cells separated by circular arcs that meet at equal angles of 120°. The 2D structures, shown in figure 1, can be viewed as cross sections of 3D honeycombs. All lines, which represent liquid films with zero thickness, have equal length in a perfectly ordered foam that is undeformed. Cell 'volumes' and edge lengths vary in the polydisperse hexagonal structure, but all edges are straight indicating that each cell has the same internal pressure. All cells do not have six sides in the disordered structure, which has curved edges and different pressures.

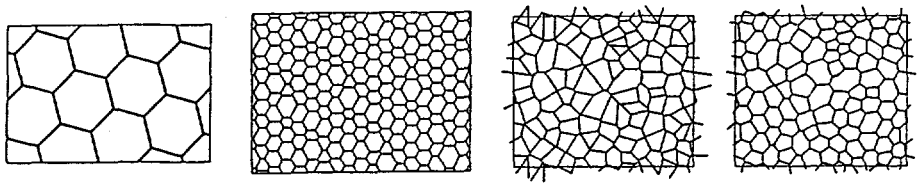

Figure 1. Perfectly ordered honeycomb, polydisperse hexagons, Voronoi polygons, which do not satisfy Plateau's laws, and disordered foam produced by relaxing Voronoi polygons.

3.2. LIQUID FOAMS

Princen [7] pioneered the microrheology of 2D foams. Khan & Armstrong [8] derived the shear stress σ for a perfectly ordered foam in simple shear

$$\sigma = \frac{G\,\gamma}{\sqrt{1+\gamma^2/4}}\,, \qquad G = \frac{3^{1/4}}{\sqrt{2}}\,\frac{T}{V^{\frac{1}{2}}} = 0.931\,\frac{T}{V^{\frac{1}{2}}} \tag{2}$$

where G is shear modulus, γ is shear strain, T is interfacial tension, and V is the cell 'volume.' This result deserves several comments. The shear stress does not depend on the foam orientation so the *nonlinear* elastic response is *isotropic*; hexagonal symmetry alone only guarantees isotropic *linear* elastic response. The shear modulus, as well as the stress and energy density, scale as $T/V^{\frac{1}{D}}$ where D is the dimension and $V^{\frac{1}{D}}$ is a characteristic cell size. A soap froth with smaller cells is stiffer.

Equation (2) applies up to strains where some film length goes to zero, which creates an unstable situation with film connectivities of four. This triggers topological transitions called $T1$s that cause discontinuities in the energy and stress-strain curve. The first $T1$ determines the elastic limit; the corresponding stress and strain depend on orientation of the foam. For certain orientations, the foam structure and stress are periodic functions of strain for simple shear and planar extensional deformations [9, 10]. The average stress $\langle\sigma\rangle$ for each strain-periodic condition corresponds to the dynamic yield stress. The stress-strain curves for the perfectly ordered foam exhibit large fluctuations and $\langle\sigma\rangle$ is very sensitive to orientation.

The energy (edge length) density of a polydisperse hexagonal foam with average cell volume V is identical to that of a perfectly ordered foam; consequently, the elastic behavior is the same [11]. The strain energy function $\mathcal{W}$ that describes this nonlinear elastic response is given by

$$\mathcal{W} \;=\; 2\,G\,(\lambda_1+\lambda_2) - P_b(1-\phi)\log(\lambda_1\lambda_2-\phi) \tag{3}$$

where the λ_i are principal stretch ratios, P_b is the bubble pressure in the undeformed foam, and ϕ is the volume fraction of liquid. Equation (3) is

valid as long as the foam structure remains polydisperse hexagonal. For a dry foam (ϕ=0) this means that all film lengths remain finite so there are no topological changes that are precipitated by unstable edge connectivities of four. A wet foam (ϕ>0) remains polydisperse hexagonal as long as no film length *in between* Plateau borders goes to zero.

For isochoric deformations such as simple shear, where the foam volume does not change, the product $\lambda_1\lambda_2$ is unity; consequently, the shear modulus G does not depend on liquid content ϕ. This lack of dependence on ϕ can be explained by considering the threefold Plateau borders where liquid collects at the cell corners. These Plateau borders translate and rotate as the foam deforms but they do not change shape, therefore, they do not contribute to the strain energy since their interfacial 'area' does not change with deformation. It is ironic that nonlinear response of the polydisperse hexagonal foam is isotropic even though polydispersity breaks the hexagonal symmetry that guarantees isotropic linear response.

The complete lack of dependence between G and ϕ also holds for disordered 2D foams as long as all Plateau borders form threefold junctions between films, which only occurs near the dry limit. The decoration theorem of Bolton & Weaire [12] sheds additional light on this situation. The equilibrium structure of a wet foam can be regarded as a dry foam whose vertices have been decorated with threefold Plateau borders. The dry foam can be constructed by continuing the circular arcs, which represent films, into the Plateau borders where they meet at 120°. Plateau borders increase in size as ϕ increases and eventually merge with neighbors to form higher connectivity junctions. The continued arcs in such structures do not meet at 120°; the connectivity of film junctions and the stress both depend on ϕ. Simulations indicate that G decreases with increasing liquid content when the decoration theorem does not apply [13, 14]. Eventually, bubbles lose contact with neighbors and become circular beyond the percolation limit where G is zero.

3.3. CELLULAR SOLIDS

We now consider solid foams where the cell structure is patterned after liquid foams. Just imagine that liquid films are transformed into solid struts by some chemical or thermal process. The in-plane elastic constants of a regular honeycomb are given by

$$K_h = \frac{1}{4\sqrt{3}\,\mathcal{M}}\,, \qquad G_h = \frac{1}{2\sqrt{3}\,(\mathcal{M}+\mathcal{N})} \tag{4}$$

where K_h is the bulk modulus and G_h is the shear modulus [15]. The parameters $\mathcal{M}$ and $\mathcal{N}$ are compliances that relate strut-level forces and

displacements due to stretching and bending. The undeformed struts have mirror symmetry about their axis and midpoint. The compliances can be evaluated for various strut shapes but we only consider struts with uniform thickness. The volume fraction of solid ϕ is often referred to as the relative foam density. For low-density foams where $\phi \ll 1$, $\mathcal{M}^{-1} = \sqrt{3}\, E\phi \gg \mathcal{N}^{-1} = 3\sqrt{3}/4\, E\phi^3$, where E is Young's modulus of the solid material in the struts. The inequality emphasizes that long slender struts are much easier to bend than to stretch. The elastic constants evaluate to

$$K_h = \frac{1}{4}\, E\, \phi\,, \qquad G_h = \frac{3}{8}\, E\, \phi^3\,. \tag{5}$$

Both moduli scale with E. In sharp contrast with liquid foams, the stiffness of cellular solids does not depend on cell size; the moduli are identical for self-similar structures. The bulk modulus is order ϕ because hydrostatic loading only induces axial strut displacements. The shear modulus is order ϕ^3 because strut bending is the dominant mechanism when $\phi \ll 1$.

The strut lengths and the corresponding strut-level compliances vary in a polydisperse hexagonal cellular solid, so analytic solutions are not feasible. Force and moment balances and compatibility conditions provide a system of $11N$ algebraic equations that are solved numerically to evaluate effective elastic response. We only consider struts with uniform thickness but distinguish two cases: constant strut thickness (CT) throughout the foam, and constant strut mass (CM), which means that strut length×thickness does not vary. In general, the elastic behavior is not isotropic, however orientation dependence is rather mild and decreases with N, as expected. All results are averaged over foam orientation.

Polydispersity does not change the bulk modulus K_{CT} when all of the struts have the same thickness because joint displacements are affine, and each strut carries the same axial load as the perfectly ordered foam. The results for the constant-strut-mass case are represented very accurately by $K_{CM} = K_h/(1+\mu_2)$, where $\mu_2 = N^{-1}\sum[(L/\overline{L}) - 1]^2$ is the second moment of the strut-length distribution. The joint displacements are not affine however bending is negligible. The axial load in each strut is reduced by a factor of $(1+\mu_2)$; this can be calculated by assuming that all of the struts, which have different length but the same mass, are connected in series.

The shear modulus for constant-strut-thickness is well represented by $G_{CT} = G_h\,(1+\mu_2)$, which indicates that polydispersity increases stiffness. In constrast, G_{CM} decreases very slightly with μ_2. We can not offer a simple explanation for the effect of polydispersity on the shear modulus.

The moduli of solid foams do not scale with cell size; however, they do depend on the distribution of cell size as well as on the distribution of material within the network of struts. With this in mind, we note that

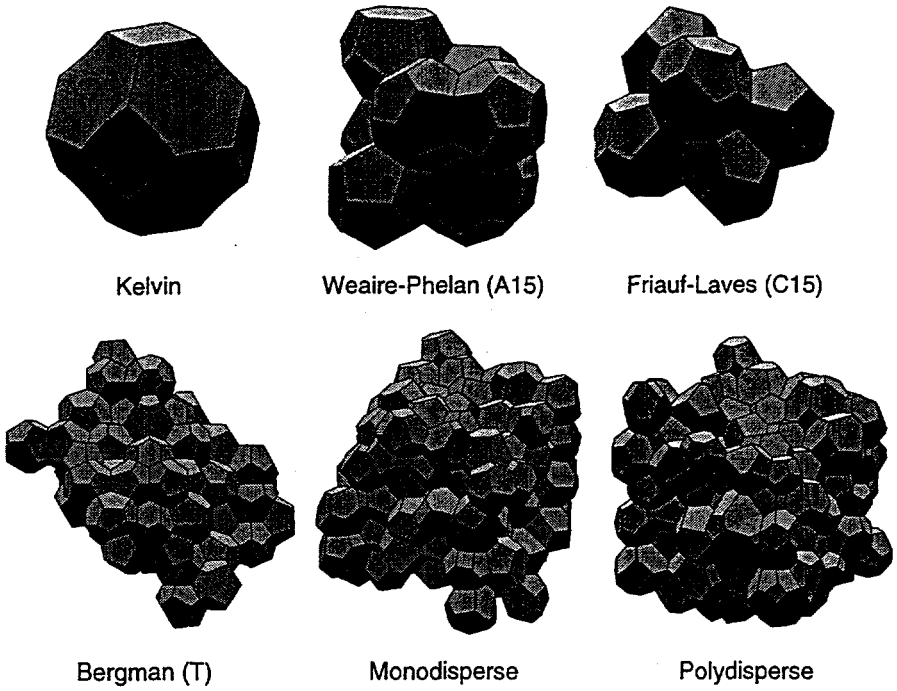

Figure 2. Kelvin cell, three TCP structures, and two random foams.

experimental data, which appear to support a correlation between foam modulus and cell size, could actually be explained by systematic variations in cell-size distribution or cell-level material distribution. Viscous and surface tension effects interact when bubbles grow and deform during foam formation. These effects exhibit different scaling with bubble size that can cause systematic variations in foam structure with cell size.

4. Three Dimensions

4.1. LIQUID FOAMS IN THE DRY LIMIT

4.1.1. *Cell Structure*

A dry soap froth based on the Kelvin cell [16] is the only perfectly ordered structure known that is consistent with Plateau's laws. This establishes the Kelvin foam as a natural starting point for developing micromechanics models in 3D, just like the honeycomb in 2D. The Kelvin cell and other foam geometries are shown in figure 2.

The discovery of the elegant Weaire-Phelan (WP) structure [17] was a watershed event in foam research. Its impact goes beyond providing a counterexample to Kelvin's candidate for the most efficient division of space

into equal-volume cells. Weaire and Phelan brought Ken Brakke's Surface Evolver computer program [18] to the attention of the foam community. The Surface Evolver is publically available from the Geometry Center at the University of Minnesota (by anonymous ftp from geom.umn.edu); it has been used to study a wide range of problems involving surfaces shaped by surface tension and other energies. The Surface Evolver was used to compute all of the liquid foam geometries discussed in this section.

The Weaire-Phelan phenomenon has also stimulated a search for monodisperse foams with even lower energy. Rivier [19] has pointed out that WP is one of two dozen or so structures known as tetrahedrally close-packed (TCP) to crystallographers and Frank-Kasper to metallurgists and materials scientists. TCP foams are restricted to four polyhedra having 12, 14, 15, or 16 faces. Each n-hedron has 12 pentagonal faces and $n-12$ hexagonal faces. The TCP structures shown in figure 2 include Weaire-Phelan (A15), Friauf-Laves (C15), and Bergman (T), all of which have cubic symmetry. This high symmetry is convenient because one only has to probe in two principal directions to determine orientation dependence of elastic properties [20].

Voronoi polyhedra produced from random points in a unit cell have the proper connectivity of a soap froth but they do not have minimal surface area. We have used the Surface Evolver to relax Voronoi partitions of space. Consider the analogous 2D problem (figure 1). Each Voronoi cell associated with a random seed consists of all points closer to that seed than to any other. The edges of a Voronoi polygon lie on perpendicular bisectors between neighboring seeds; but the straight edges do not meet at 120°. During the relaxation process, vertex positions and edge curvatures are adjusted until pieces of circles meet at equal angles and satisfy constraints on cell volumes. Relaxation also involves topological changes ($T1$s) that are triggered by edges going to zero length. Many cell neighbors and edges switch in going from Voronoi cells to minimal structures.

In 3D, Voronoi polyhedra have flat faces and straight edges. No Voronoi partition can satisfy Plateau's law requiring each edge to meet at equal angles because no polygon with straight edges has all vertex angles equal to the tetrahedral angle. As the surface evolves during relaxation, cell edges shrink and trigger topological transitions.

Voronoi polyhedra were computed with a program written by John Sullivan. The initial Voronoi seeds were generated by two methods: random sequential adsorption (RSA) and random close packing (RCP) of hard spheres. In RSA, a randomly generated seed is accepted in the unit cell only if the distance to existing seeds is greater than some diameter, which is chosen to be as large as possible to pack N spheres in a cube with spatially periodic constraints. Relatively loose packings of monodisperse

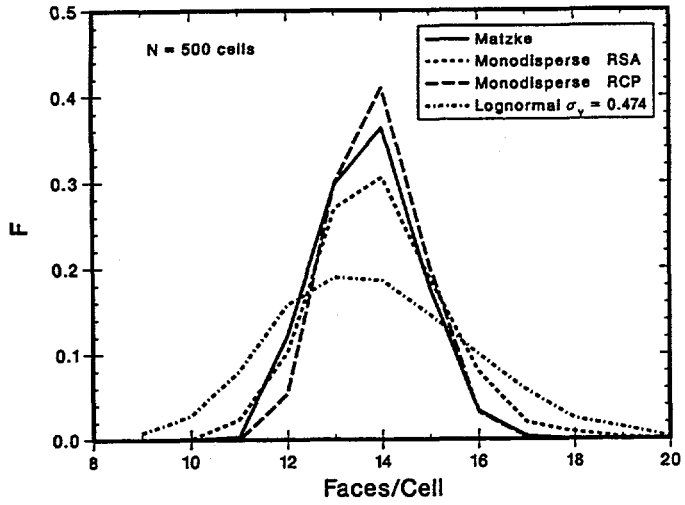

Figure 3. Distribution of polyhedra with n faces in random foams.

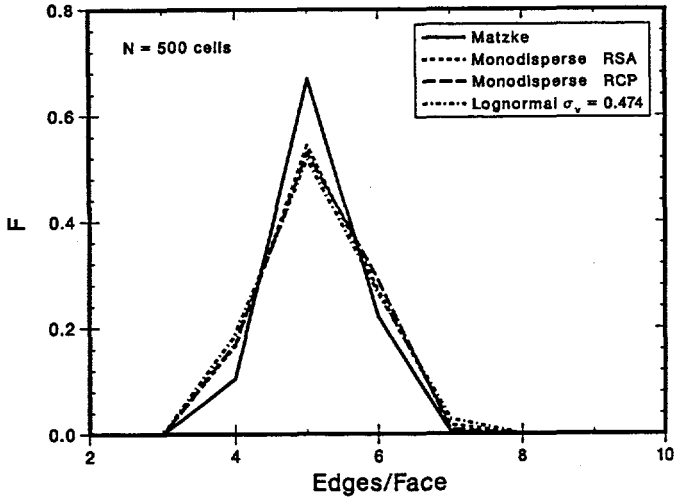

Figure 4. Distribution of faces with p sides in random foams.

spheres with volume fractions up to ϕ_s=0.35 were achieved with N=512. Molecular dynamics simulations, using software provided by Frank van Swol, produced much denser configurations with ϕ_s=0.64. The standard deviations on Voronoi polyhedra volumes were about σ_v=0.13 for RSA and σ_v=0.04 for RCP.

Typical distributions of polyhedra with n faces and polygons with p sides, are shown in figures 3 and 4. These results are compared with experimental observations by Matzke [21] on six hundred bubbles in foams

that were believed to be monodisperse. The computed statistics for relaxed monodisperse foams are in substantial agreement with the experimental data. Matzke found averages of 13.70 faces/cell and 5.124 edges/face. We performed eight relaxation simulations on Voronoi partitions based on RCP with N=500, 512 and found 13.85 faces/cell and 5.133 edges/face.

Triangular faces are common among Voronoi cells but very rare in monodisperse soap froths; Matzke did not find any three-sided faces. Nor did he find a single Kelvin cell in his experiments, although others have. We found a few Kelvin cells among our relaxed structures but they were very rare, which is not surprising since pentagonal faces are so common. The Voronoi foams based on RSA have broader distributions of polyhedra and polygons than those based on RCP, which are much closer to the final relaxed systems.

Relaxed foams with lognormal distribution of cell volumes were simulated to show the effects of polydispersity; in the most polydisperse, $\sigma_v = 0.474$, individual cell volumes ranged from 0.224 to 3.65 with an average of one. The distribution of n-faced polyhedra, shown in figure 3, is obviously broader for the polydisperse system, which even contained cells with 20 to 23 faces that were absent in the monodisperse foams. Larger polyhedra tend to have more faces and smaller polyhedra tend to have fewer faces. By contrast, the distribution of p-sided faces, shown in figure 4, is surprisingly similar for the polydisperse and monodisperse structures. Clearly, this would not be expected in a polydisperse foam that contains a large number of extremely small cells; tetrahedra would be common.

Two geometric properties, surface area and edge length, are graphed in figure 5 for several types of relaxed foams. Both quantities fall in a relatively narrow range for monodisperse systems. The polydisperse foams have significantly lower area and edge length than the others. Different size bubbles pack more efficiently, just like different size spheres.

4.1.2. *Shear Modulus*

The shear moduli of various monodisperse foams are given in Table 1. All of the structures except the random foams have cubic symmetry, so orientation dependence of the shear modulus is evaluated by applying two specific deformations [22], which give two distinct shear moduli

$$G_1 = \frac{1}{2}\,(c_{11} - c_{12})\,, \qquad G_2 = c_{44} \tag{6}$$

where the c_{ij} are elastic constants used by Love [1] and Nye [20]. An effective isotropic shear modulus $\overline{G}$ is calculated by averaging G over foam orientation. We use the Voigt average, which is performed at constant strain. The Kelvin foam is significantly more anisotropic than the TCP foams.

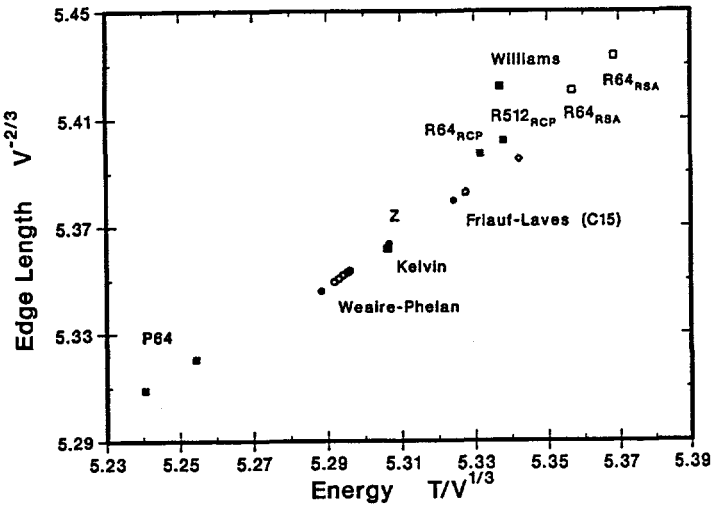

Figure 5. Cell edge length graphed against interfacial energy for dry foams with minimal surface area. The label 'R' refers to random, monodisperse structures and 'P' refers to random, polydisperse structures.

The T foam, which has many faces of different orientation, is essentially isotropic. As measured by $\overline{G}$, our results for monodisperse structures fall in a relatively narrow range, but the TCP foams are perceptibly stiffer than the Kelvin and random foams. The influence of polydispersity on the shear modulus of disordered foams is currently under study.

TABLE 1. Shear moduli of dry foams

Foam structure	G_1	G_2	$\overline{G}$
Kelvin	0.5706	0.9646	0.8070
Weaire-Phelan (A15)	0.8902	0.8538	0.8684
Friauf-Laves (C15)	0.8448	0.8860	0.8695
Bergman (T)	0.858	0.856	0.857
Random (monodisperse)			0.78 ± 0.08

The bidisperse Wearie-Phelan foams, shown in figure 6, represent a simple model system that is polydisperse [23]. The unit cell contains six 14-hedra with volume V_{14} and two pentagonal dodecahedra with volume βV_{14}; these particular volume constraints preserve cubic symmetry. This system exhibits counter-intuitive results for bubble pressure: the pressure inside the dodecahedra is always greater than the pressure inside the 14-hedra,

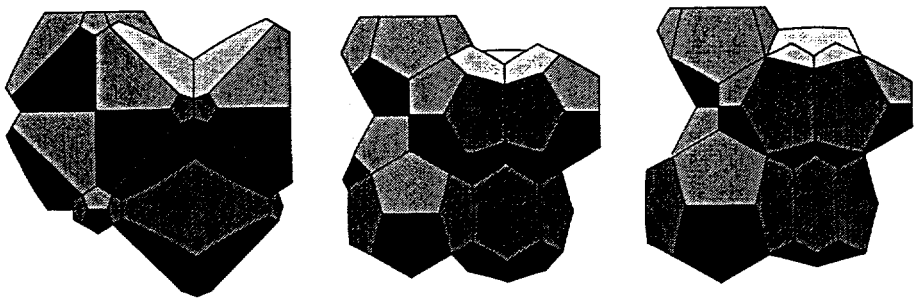

Figure 6. Bidisperse Wearie-Phelan foams with $\beta = 0.04, 1.0, 2.4$.

even when the dodecahedra are larger. The pressure difference $P_{12}-P_{14}$ decreases but remains positive as β increases. In contrast with isolated soap bubbles, the pressure inside foam cells depends on their size and topology. The interfacial energy density increases with β; this is consistent with diffusion-driven coarsening because the total energy of the foam decreases as gas diffuses from the higher pressure dodecahedra into the tetrakaidecahedra. The total cell edge length per unit volume also increases with β. The shear moduli of bidisperse WP foams were evaluated over the range $0.04<\beta<2.4$. The effective isotropic shear modulus $\overline{G}$ varies less than 0.4% from the monodisperse case over the entire range of β, which indicates that the shear modulus is relatively insensitive to bidispersity.

4.1.3. *Large Extensional Deformation*

We now focus on large deformations of a Kelvin foam. Consider uniaxial extension in a $\langle 100 \rangle$ direction with no volume change [24, 25]. This is the most symmetric distortion of a perfectly ordered foam. The evolution of cell geometry and tensile stress with Hencky strain ϵ are shown in figure 7. The area of the 'square' face that is being pulled decreases with increasing strain but remains finite in the limit $\epsilon \rightarrow \epsilon_{T1}=0.254$. Beyond ϵ_{T1}, no stable solution satisfies Plateau's laws and maintains contact between the original cell neighbors. This situation triggers a topological transition ($T1$), which marks the limit of reversible elastic behavior and the onset of plasticity.

The stress-strain curve exhibits a maximum in the tensile stress and a turning point. The unstable solutions on the curve below the turning point have the same topology but higher surface area than their stable counterparts. The unstable solution at $\epsilon=\frac{1}{3}\log 2=0.231$, where the tensile stress is zero, corresponds to a rhombic dodecahedron on a face-centered-cubic (fcc) lattice, which will be discussed later.

In view of the cost of computing minimal surfaces, it is useful to consider solutions based on oversimplified foam geometry. In all three approxima-

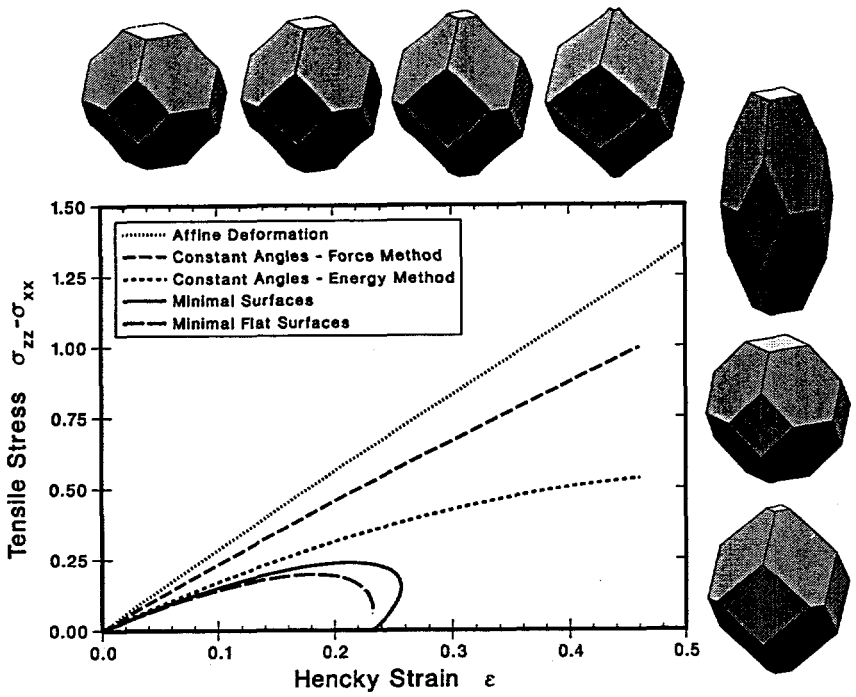

Figure 7. Evolution of cell geometry and tensile stress for uniaxial extension in a ⟨100⟩ direction. The horizontal sequence of minimal structures can be compared with approximate geometries with flat faces. The highly stretched cell corresponds to affine deformation.

tions to be considered, the undeformed cell is a regular tetrakaidecahedron; the faces remain flat as the foam deforms but the dihedral angles are different in each case. Under affine deformation, all points in the foam move exactly with the macroscopic strain. The pulled square continues to shrink for all values of strain (figure 7) but there is no criterion for topological transition so there is no elastic limit. The affine assumption gives the largest tensile stress. Next, we assume constant dihedral angles that do not vary with strain. The pulled square shrinks to zero area when $\epsilon=\frac{2}{3}\log 2=0.462$ causing edge connectivity of eight, which violates Plateau's laws and triggers a $T1$. There are two different stress-strain curves in figure 7, which correspond to different methods for calculating the stress. The force and energy methods give different results in this situation where film-level forces are not balanced and energy is not minimized. In the third approximation, dihedral angles are determined by minimizing the total surface area of all the flat faces. The evolution of foam structure and stress are qualitatively

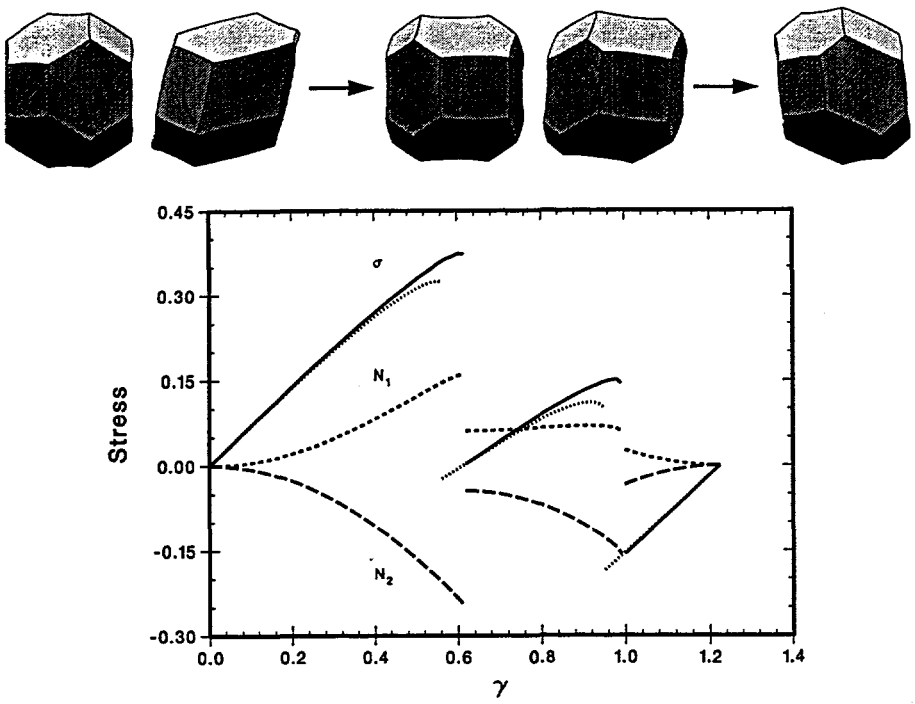

Figure 8. Evolution of cell geometry, shear stress, and normal stress differences for simple shearing flow. This cell orientation has the smallest strain period $\gamma_p=(3/2)^{1/2}$. The dotted curve refers to the minimal planar approximation.

similar to the complete solution; the stress exhibits a local maximum and a turning point but is lower. Results for this case indicate that approximate solutions do not necessarily provide bounds for exact solutions.

4.1.4. *Simple Shearing Flow*

Under simple shearing flow, the structure and stress of a Kelvin foam are piecewise continuous functions of shear strain γ [26]. Each discontinuity corresponds to a topological change that is preceded by shrinking faces. Each $T1$ reduces surface energy, results in cell-neighbor switching, and provides a cell-level mechanism for plastic yield behavior during foam flow. In figure 8, the foam is oriented so that structure and stress are periodic functions of strain.

There are two $T1$s per cycle; each is triggered by opposite edges of shrinking quadrilateral faces going to zero length, which leads to unstable connectivity. This *standard* transition is very different from the *point* transition in the extensional deformation, where all edges on a face shrink together. Symmetry imposes strong restrictions on the type and outcome

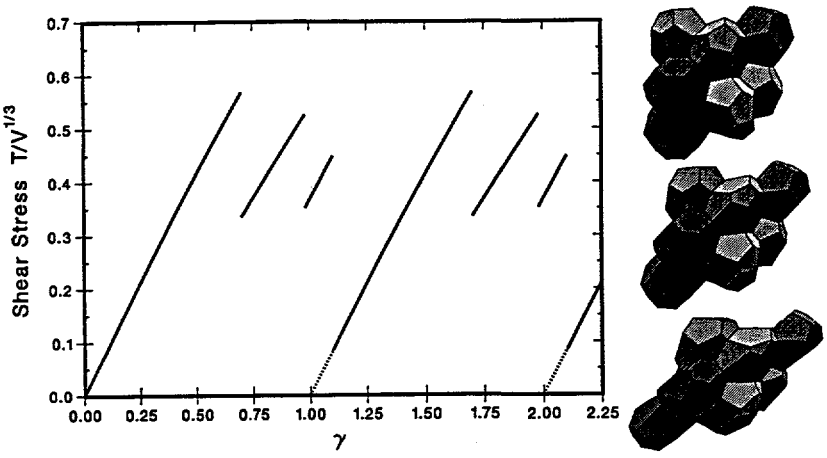

Figure 9. Shear stress versus shear strain for simple shearing flow of a Weaire-Phelan foam. This cell orientation has the smallest strain period γ_p=1.

of topological transitions when the foam is perfectly ordered. Kelvin cells beget Kelvin cells.

TABLE 2. Topology changes for a Weare-Phelan foam in simple shearing flow

	Faces					Polyhedra							
γ	4	5	6	7	8	d	D	x	X	y	Y	z	Z
0-0.7	0	48	6	0	0	12	12	14	14	14	14	14	14
0.7-0.98	14	22	18	2	0	18	16	12	12	13	13	14	14
0.98-1.1	17	20	16	4	1	16	16	14	14	14	14	14	14
1.1-1.7	0	48	6	0	0	12	14	14	14	14	14	12	14

A Weaire-Phelan foam has less symmetry and exhibits more diverse topological transitions than a Kelvin foam in simple shearing flow. Table 2 contains statistics on the outcome of topological transitions that correspond to the stress-strain curve in figure 9. Up to γ=0.70 where the first $T1$ occurs, there are only pentagonal and hexagonal faces, which is characteristic of TCP foams. The first $T1$ *eventually* produces 4-sided and 7-sided faces, the total number of faces increases from 54 to 56, the original dodecahedron 'd' gains faces to become an 18-hedron, *etc.* We say 'eventually' because this structure is not achieved in a single step. A local topology change that corrects an unstable condition leads to other edges vanishing and induces another topology change, *etc.* The cascade of $T1$s that occurs at γ=1.10 involves at least nine steps before the structure regains

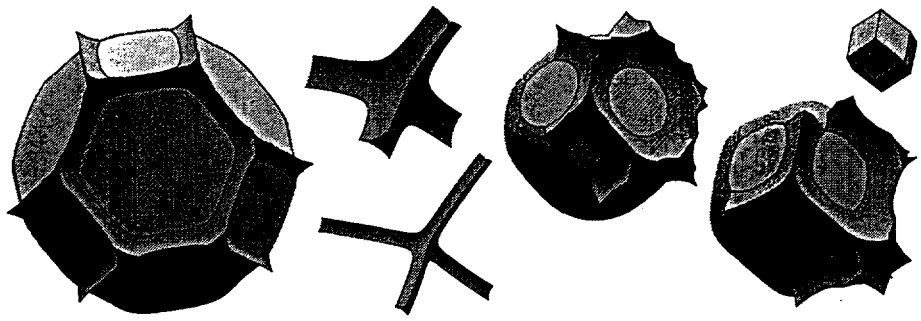

Figure 10. Wet Kelvin cells, ϕ=0.01, 0.06; a wet rhombic dodecahedron, ϕ=0.06; Plateau border segments from a Kelvin cell, ϕ=0.001, 0.01; and a rhombic dodecahedron.

Weaire-Phelan topology and begins a new stress-strain cycle; but notice that bubbles have changed identity: an original dodecahedron has become a 14-hedron and *vice versa*. Bubbles have shuffled within the lattice.

4.2. WET FOAMS

The Surface Evolver can also be used to study the structure and microrheology of wet foams (and liquid-liquid emulsions) for which the volume fraction of continuous phase ϕ is finite [27]. We consider the case where all of the liquid (continuous phase) collects in Plateau borders that form interconnected channels along bubble 'edges' where films join. Assuming dry films corresponds to physical situations where film thickness is negligible compared to the cross section of Plateau borders. The distribution of liquid between the films and borders is set by a balance between disjoining pressure and Laplace pressure.

A wet Kelvin cell with ϕ=0.01 is shown in figure 10. The Plateau border interfaces have tension T and the films have tension $2T$ from two interfaces. The bubble and border have volume (1-ϕ)V and ϕV, respectively. Figure 10 illustrates an important fact about the geometry of Plateau borders and the analogous struts in a solid foam with open cells, which will be discussed in Section 4.3. When $\phi \ll 1$, the borders can be considered long and slender and the size of the junction can be neglected; however, ϕ=0.01 might not always be small enough for these asymptotic conditions to give accurate results.

Unlike the dry limit, a perfectly ordered wet foam can have more than one stable structure, *e.g.*, bubbles compressed on a face-centered-cubic (fcc) lattice, which relate to closest packed spheres (figure 10). The polyhedron associated with fcc packing, the rhombic dodecahedron (RD), has twelve

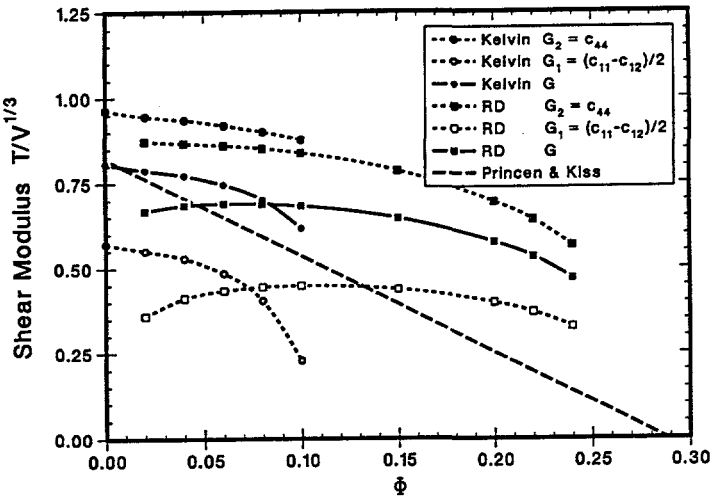

Figure 11. Shear moduli for wet Kelvin and wet rhombic dodecahedron foams compared with the empirical relation of Princen & Kiss.

identical rhombic faces. The obtuse angle of these faces equals the tetrahedral angle, and the vertex shares four edges, so Plateau's laws are satisfied locally. However, a dry foam with rhombic dodecahedral cells is unstable because eight edges meet at the corners with acute angles. Plateau's laws do not pertain to wet foams. The connectivity of Plateau borders can exceed four in wet foams, which gives a richer variety of topologies than in dry foams.

The shear moduli for wet Kelvin and wet RD foams are graphed in figure 11 and compared with the empirical correlation of Princen & Kiss [28], obtained from data for concentrated oil-in-water emulsions with polydisperse drop-size distributions. Note that in the dry limit this correlation extrapolates to a value that is consistent with the results in Table 1. Both wet structures have positive G_i and are stable over some overlapping range of ϕ. The smaller shear modulus for the Kelvin foam decreases rapidly as $\phi \rightarrow \phi^* \approx 0.11$; at ϕ^* the smaller (original 4-sided) films shrink to zero area prior to being consumed by surrounding borders that grow with ϕ. When these borders converge to form eight-way junctions, the bubbles lose contact with all next nearest neighbors on the bcc lattice, which creates an unstable situation.

Consider the uniaxial extension described in Section 4.1.3 but applied to a wet Kelvin foam. A bcc lattice becomes fcc when $\epsilon_{fcc} = \frac{1}{3}\log 2 = 0.231$. Figure 12 shows the evolution of bubble shape with strain. At some $\epsilon_{K,RD} < \epsilon_{fcc}$, the structure undergoes a transition from wet Kelvin topology to wet RD topology, which we label $T_{K,RD}$. Films that are perpendicular to the

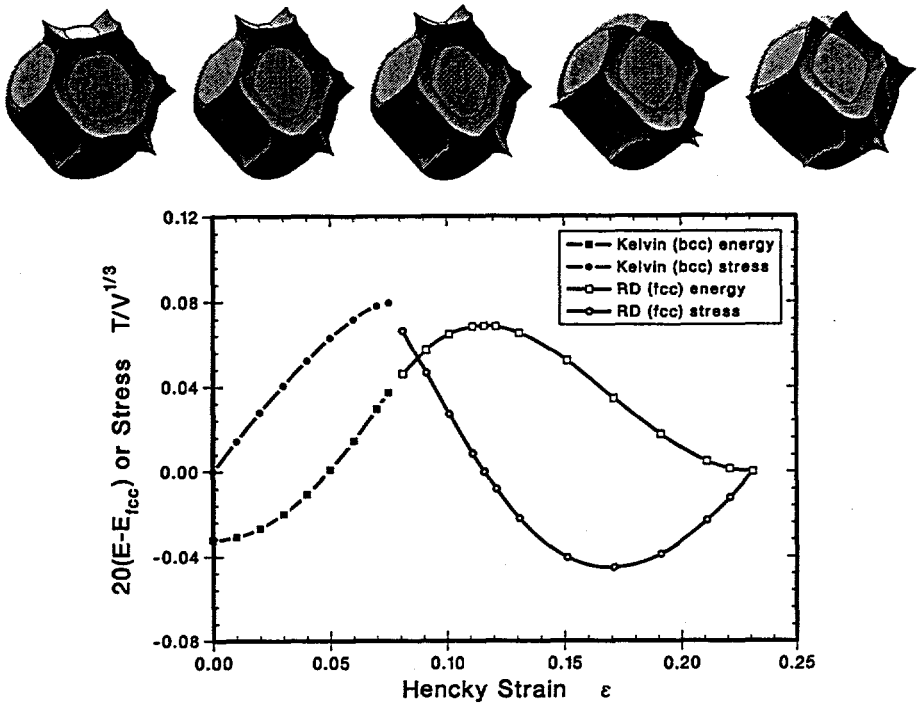

Figure 12. Evolution of bubble shape as a wet Kelvin cell on a bcc lattice stretches to a wet rhombic dodecahedron on an fcc lattice, ϕ=0.04. The cell orientation is the same as in figure 7. Graph of tensile stress and energy density, ϕ=0.06.

stretching axis shrink and eventually vanish at $\epsilon_{K,RD}$, resulting in bubbles with twelve films and some eight-way Plateau border junctions. Further stretching takes these bubbles to wet RD with isotropic stress at ϵ_{fcc}. Figure 12 shows the tensile stress σ and interfacial energy density for this process. The slope of the stress-strain curve evaluated at ϵ=0 and at ϵ=ϵ_{fcc} relates to the smaller shear modulus of each structure. The energy maximum E_{max} that occurs when the stress changes sign at ϵ_{max}, determines the energy barriers between the undeformed structures, *e.g.*, ΔE_{bcc}=E_{max}−E_{bcc}, which also represents the area under the stress-strain curve. E_{bcc} and E_{fcc} both decrease with ϕ and cross when ϕ≈0.064; E_{bcc} is lower when ϕ is small.

The process just described appears to be *completely* reversible–the wet RD foam can be compressed to a Kelvin foam. Reversibility implies that the energy and its first derivitive are continuous at $\epsilon_{K,RD}$=$\epsilon_{RD,K}$. Reversibility might be expected because of the symmetry involved. The reverse topological transition $T_{RD,K}$ involves bubbles that are aligned with the compression axis and separated by an eight-way junction, becoming neighbors. The new neighbors are separated by a film that forms where the bubbles first contact

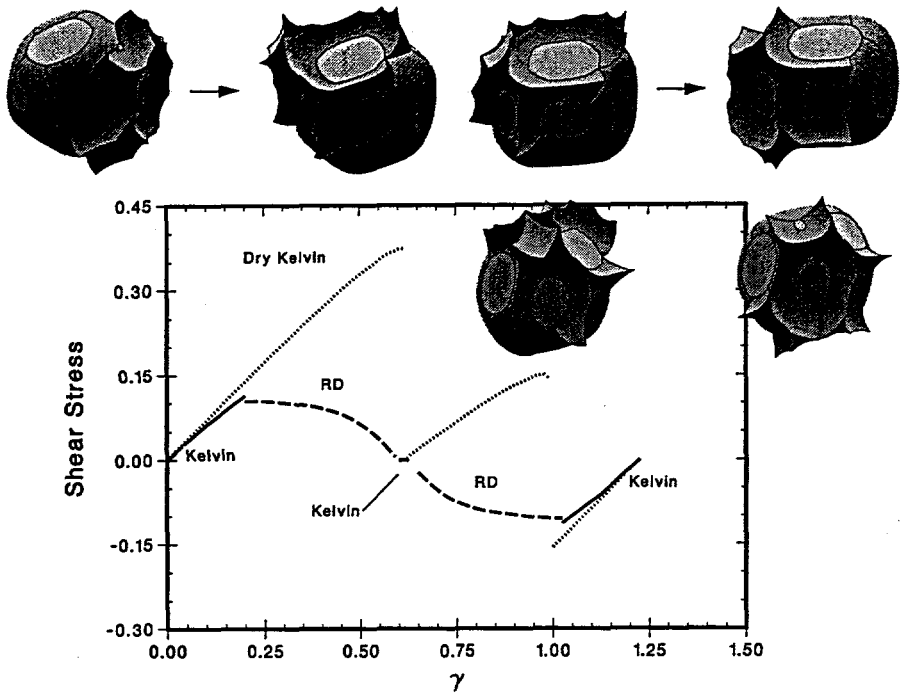

Figure 13. Evolution of bubble shape and shear stress for simple shearing flow of a wet Kelvin foam with ϕ=0.06. Cell orientation is the same as in figure 8. Topology changes from wet Kelvin to wet RD to wet Kelvin. The lower bubbles show a different view of the second transition, which involves the formation of a new film when opposite interfaces of an eight-way junction come together.

and grows in area as ϵ decreases below $\epsilon_{RD,K}$. A transition of type $T_{RD,K}$ is initiated when interfaces on opposite sides of an eight-way junction come into contact.

Both topological transitions occur in simple shearing flow but they are not reversible. Consider the flow described in Section 4.1.4 but applied to the wet Kelvin foam with ϕ=0.06. Figure 13 contains representative structures and the stress-strain curve. Instead of two $T1$s per cycle like the dry case, there are four distinct topology changes in the wet case: a $T_{K,RD}$, then a $T_{RD,K}$, then a $T_{K,RD}$, and then a $T_{RD,K}$ to complete the cycle. Both $T_{K,RD}$ transitions involve the 'same' shrinking film as the dry foam, but in each case, a stable wet RD results. Both $T_{RD,K}$ transitions involve contact between opposite interfaces of an eight-way junction. Different from the reversible uniaxial extension, the stress and energy both decrease with each transition in simple shear. The magnitude of these jumps is much smaller for the wet foam than the dry foam (figure 13). The same is true

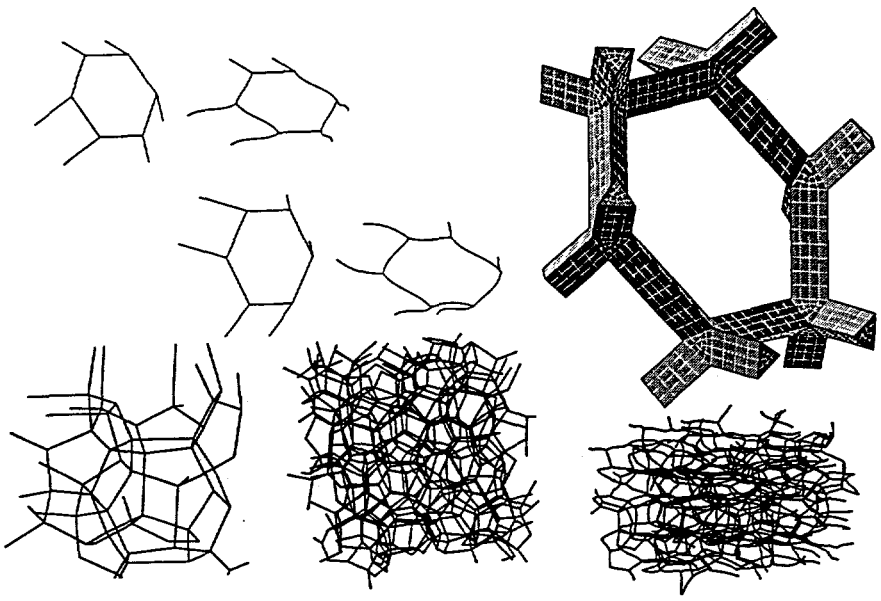

Figure 14. Beam element models for open-cell foams including: Kelvin, Weaire-Phelan, and random with N=64. Continuum element mesh for a Kelvin foam with ϕ=0.0267.

for the average shear stress $\langle\sigma\rangle$, which corresponds to the (viscometric) yield stress of the foam. Consistent with measurements of yield stress by Princen [29], $\langle\sigma\rangle$ decreases very rapidly with ϕ.

When ϕ is very small, we anticipate that wet RD structures will be unstable intermediates that lead to wet Kelvin structures. There will be two Kelvin branches in the stress-strain cycle, just like the dry limit.

4.3. SOLID FOAMS WITH OPEN CELLS

In nature and industry, liquid foams undergo phase changes to produce solid foams so the cell-level structure of the former heavily influences the latter. This justifies and motivates using the geometry of soap froth and related materials as templates for developing micromechanics models for cellular solids.

4.3.1. *Linear Elastic Behavior of a Kelvin Foam*

A low-density Kelvin foam with open cells is composed of identical, straight struts of length $2\mathcal{L}$ that meet at identical, rigid joints. Force-displacement relations at the strut level are expressed through compliances for stretching $\mathcal{M}$, bending $\mathcal{N}$, and twisting $\mathcal{J}$. Analytic solutions for arbitrary homogeneous deformations of the foam provide all forces, moments, and displace-

ments at the strut level, and the rotation at each joint [30]. The effective elastic constants of the foam include the bulk modulus K and two shear moduli, which take the form

$$\begin{aligned} K &= \frac{1}{24\sqrt{2}\,\mathcal{L}\,\mathcal{M}} \\ G_1 &= \frac{1}{4\sqrt{2}\,\mathcal{L}\,(\mathcal{M}+3\mathcal{N})} \\ G_2 &= \frac{1}{8\sqrt{2}\,\mathcal{L}\,(\mathcal{M}+\mathcal{N}+\mathcal{L}^2\mathcal{J})} \,. \end{aligned} \tag{7}$$

The bulk modulus only depends on $\mathcal{M}$; struts neither bend nor twist when this highly symmetric structure experiences hydrostatic compression. Bending and twisting are the dominant strut-level deformation mechanisms for foams under shear because $\mathcal{M} \ll \mathcal{N}$ when the foam density ϕ is small. The modulus G_1 corresponds to compression along a $\langle 100 \rangle$ axis (pushing on squares); the absence of $\mathcal{J}$ indicates that struts do not twist (figure 14). The modulus G_2 corresponds to compression along a $\langle 111 \rangle$ axis (pushing on hexagons); struts bend and twist. Beam theory can be used to evaluate the compliances

$$\mathcal{M} = \frac{\mathcal{L}}{EA} \,, \qquad \frac{1}{\mathcal{L}\mathcal{N}} = \frac{3EI}{\mathcal{L}^4} \,, \qquad \mathcal{L}^2\mathcal{J} = \frac{1}{2}\mathcal{N}(1+\mathcal{G}) \tag{8}$$

where E is Young's modulus of the material in long slender struts with uniform cross section of area A, radius of gyration q, and moment of inertia $I{=}q^2A$. The elastic constants for the foam become

$$K = \frac{1}{9}\,E\,\phi \,, \qquad G_1 = \frac{16\sqrt{2}}{9}\,E\,(\frac{q^2}{A})\,\phi^2 \,, \qquad G_2 = \frac{G_1}{1+\mathcal{G}/3} \tag{9}$$

when $\phi \ll 1$. The parameters q^2/A and $\mathcal{G}$ depend on the strut cross section. Shapes of interest include circle, equilateral triangle, and Plateau border, which corresponds to the space between three identical, mutually tangent circles. The elastic response of the foam is isotropic ($G_1{=}G_2$) when $\mathcal{G}{=}0$, which occurs for circular struts with a Poisson's ratio ν of zero. Incompressible struts with Plateau border shape cause the most anisotropy: $\mathcal{G}{=}2/13$, $G_1{=}0.336E\phi^2$, $G_2{=}0.320E\phi^2$. An open-cell Kelvin foam exhibits weak anisotropy for strut shapes and material properties of interest; this insensitivity to orientation is surprising since G_2 involves twisting but G_1 does not.

The effective isotropic Young's modulus $\overline{E}$ for incompressible struts with Plateau border shape is

$$\overline{E} = 0.979\;E\;\phi^2 \,. \tag{10}$$

Gibson & Ashby [4] chose a coefficient of one to correlate experimental data. The coefficient in (10) is 40% smaller for circular struts.

Zhu *et al.* [31, 32] have performed an independent analysis of the linear problem under consideration and used the Elastica approach to analyze uniaxial compression at finite strains.

4.3.2. *Large Deformation Behavior: Finite Element Analysis*
Foams composed of nonlinear material, which is arranged to form a complex cell structure, are subjected to large deformations in a wide range of applications. A standard industrial test involves foam compression between two flate plates. A variety of finite element techniques are well suited for solving micromechanics problems that are relevant in these situations.

Beam Elements The primary microstructural feature found in low-density open-cell foams is the network of slender struts that meet–most often with a connectivity of four–at joints. Beam elements can be used to discretize the struts along their axis. We use the B31 beam elements that are contained in ABAQUS, a general purpose finite element program [33]. The struts in an undeformed foam are assumed to have uniform cross section and a straight axis, but these approximations can be relaxed. The location of joints and the connectivity of struts are based on the foam geometries described in Section 4.1.1; these include perfectly ordered, TCP, and random structures. Beam section properties are chosen according to the strut shape and the relative foam density, which is calculated from $\phi = \mathcal{V}^{-1} \sum_{i=1} A_i \mathcal{L}_i$, where A_i and $\mathcal{L}_i$ are the section area and length of strut i. The geometry and deformation of the joint region are neglected in the simplest beam models, which focus entirely on the mechanics of connecting struts.

Consider situations where a foam is subjected to uniaxial compression without confining the sides. The shear stresses and lateral normal stresses are zero. Stress-strain curves for three representative structures are contained in figure 15. Calculations for ϕ=0.001, 0.01 scale with $E\phi^2$. Two curves indicate the range of orientation dependence when a foam has cubic symmetry. The results for a Kelvin foam agree with the Elastica analysis of Zhu *et al.* (private communication, N.J. Mills). The large-strain behavior of the Kelvin foam is more sensitive to orientation than the shear modulus. The Weaire-Phelan foam is stiffer than the Kelvin foam and exhibits as much anisotropy, even though it contains eight different cells. The Weaire-Phelan response is characteristic of TCP foams, except the T structure, which has 81 different cells, is significantly less anisotropic. A single curve represents the essentially isotropic behavior of two different random foams with 64 cells. The Young's modulus of the random foam is about 10% larger than the Kelvin foam; this relates to the leading coefficient in (10).

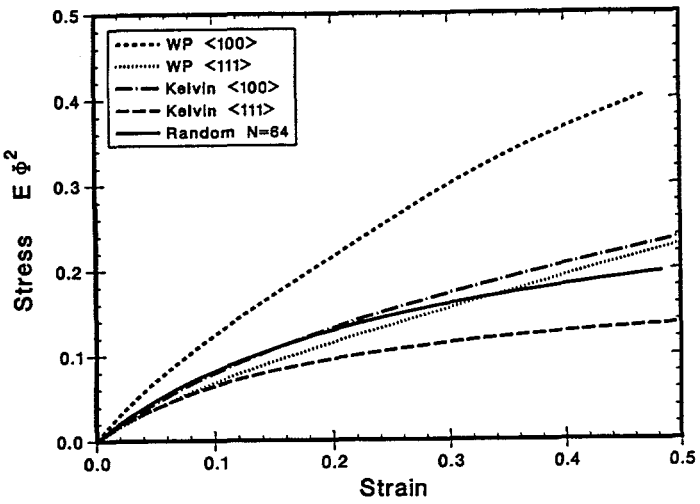

Figure 15. Stress-strain curves for Kelvin, Weaire-Phelan, and random foams under uniaxial compression.

Since the strut material is linear elastic, the significant nonlinearity of the curves in figure 15 stems entirely from large deformation of the microstructure.

In view of the simplicity of Kelvin's cell and the complexity of random foams, their macroscopic response to uniaxial compression is very similar. It is unnecessary–in some cases–to model large disordered structures, especially when perfect order will do.

The foam response is quite different for hydrostatic loading, which produces pure volume change. The pressure for the Kelvin foam is well represented by linear theory (9) up to the critical buckling load. The pressure scales as $E\phi$ because struts only carry axial loads in a *perfect* Kelvin foam. Structures that are not perfectly ordered contain struts of different length meeting at joints at different angles. Under hydrostatic loading, the struts do not experience pure axial loading and joint displacements are not affine. Off-axis loading causes strut bending and twisting at very small volume strains, which leads to the stress plateaus in figure 16. The level of these plateaus *does not* scale with $E\phi$ since bending is involved. The insert of a deformed Weaire-Phelan foam in figure 16 illustrates the strut bending generated by hydrostatic compression. The onset to the plateau is very gradual for the random foam. The plateau level in figure 16 is the same for the random and the T structure.

Recent studies of buckling instabilities, which will not be discussed here, indicate that small imperfections in the structure of Kelvin and Weaire-Phelan foams will lead to strut buckling and also produce a plateau level

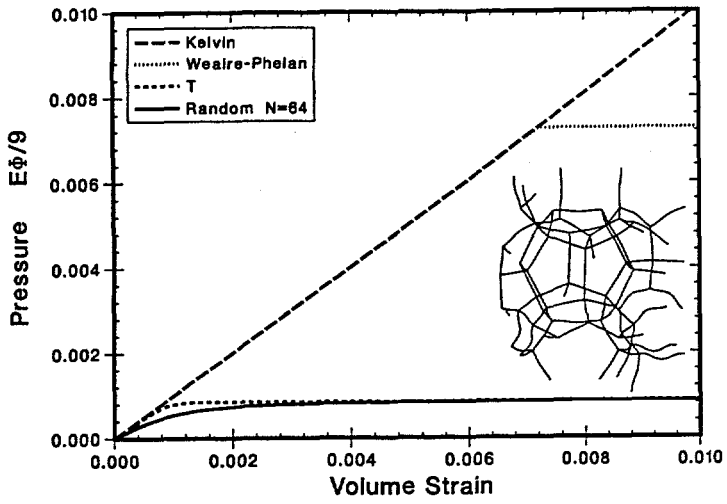

Figure 16. Stress-strain curves for Kelvin, Weaire-Phelan, T, and random foams under hydrostatic compression.

similar to the random foam.

Future analysis of hydrostatic compression and other complex load paths promises to shed more light on cell-level deformation mechanisms in foam mechanics. Large-deformation response of foams may be easier to study on a computer than in the laboratory.

Continuum Elements Struts become thicker and joint regions become larger as the density of an open-cell foam increases. Eventually, the approximations used to formulate beam elements are violated. Deformation within the joint regions also becomes more important as the distinction between joint and strut becomes more arbitrary (figure 10). Under these circumstances, continuum elements can be used to discretize the entire solid phase within the foam. This approach permits more accurate modeling of the cell-level geometry and the use of more sophisticated constitutive equations to describe nonlinear behavior of the foamed material such as viscoelasticity, plasticity, *etc.*

Figure 14 contains a continuum element mesh of an open-cell Kelvin foam with ϕ=0.0267. This corresponds to a flexible polyurethane foam with density: two pounds per cubic foot, which is often referred to as low-density. It is obvious that the struts are thick and the joints have significant volume. Computations with continuum elements are being used to study the ϕ-dependence of properties in dense foams where details of cell-level geometry are more subtle.

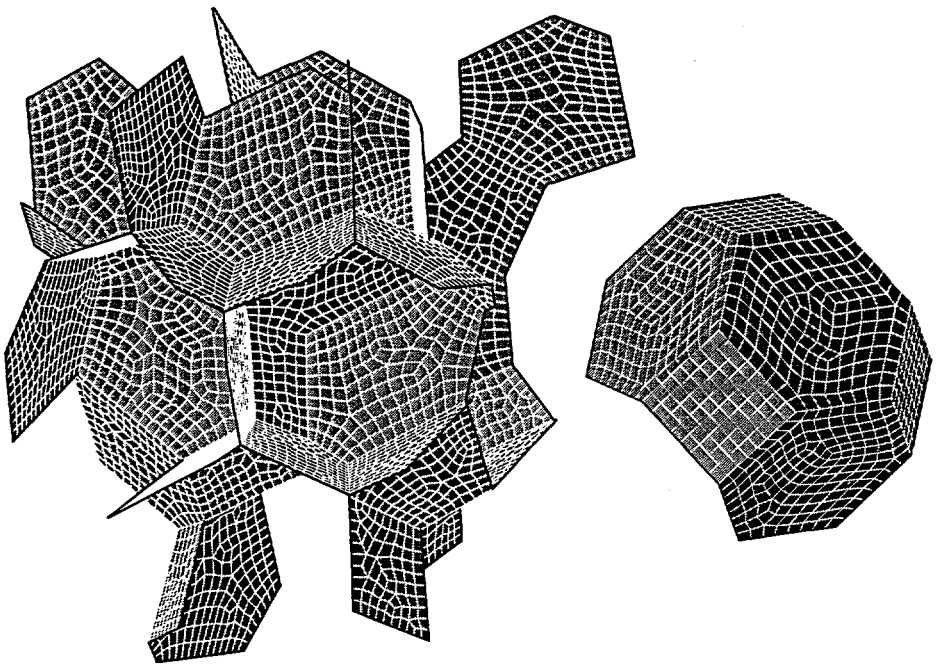

Figure 17. Shell element meshes for closed-cell Kelvin and random foam with N=10.

4.4. SOLID FOAMS WITH CLOSED CELLS

The cells in a closed-cell foam are separated from neighbors by cell walls, which are absent in an open-cell foam. We consider an extreme case where all cells are closed and all of the solid material is located in the cell walls, which is similar to neglecting the joints in a beam analysis of open-cell foams. We also assume that the cell walls are thin and flat with uniform thickness. Even with these simplifications, analytic solutions for linear elastic behavior of a Kelvin foam are not feasible. We use finite element analysis and discretize the faces with the quadrilateral shell element S4R contained in ABAQUS. With the exception of the Kelvin cell, the vertices of each face in a dry foam do not lie in a plane; therefore, we use Voronoi partitions to model the geometry of closed cell foams. Typical shell-element meshes are shown in figure 17. The Weaire-Phelan model is based on the weighted Voronoi construction of Kusner & Sullivan [34], which is monodisperse.

The elastic constants that were computed for closed-cell Kelvin and Weaire-Phelan foams with ν=0.49 for the wall material and $\phi \ll 1$ are

$$\begin{aligned} K &= 0.435\ [0.434]\ E\phi \\ G_1 &= 0.108\ [0.113]\ E\phi \\ G_2 &= 0.116\ [0.111]\ E\phi \end{aligned} \tag{11}$$

where brackets refer to Weaire-Phelan. Note that all elastic constants, even the shear moduli, scale with $E\phi$, which indicates that in-plane deformation of cell walls dominates the cell-level mechanics. This is very different from 2D where the shear modulus scales with $E\phi^3$ because cell walls bend. In 3D, each face is connected to two other faces around its entire perimeter; the resulting mechanical constraints suppress bending in the linear elastic regime.

The elastic constants for the Weaire-Phelan foam are very close to the Kelvin foam. The same is true for other structures (Friauf-Laves, a random Voronoi partition with ten cells), whose constants are not shown. All of the closed-cell foams exhibit very similar linear elastic response. It will be very interesting to see how widely this observation applies. Also different from our results for low-density open-cell foams, all of the closed-cell foams are nearly isotropic.

Hashin & Shtrikman [35] calculated upper bounds on elastic constants for two-phase solids. For low-density porous materials with ν=0.49 for the solid phase, $K_{HS} = 0.4357\ E\phi$ and $G_{HS} = 0.1996\ E\phi$. The bulk modulus of the closed-cell foams considered here is very close to the Hashin-Shtrikman bound. The shear moduli are about 50% smaller than the upper bound.

Compare the elastic constants of open-cell foams and closed-cell foams given in (9) and (11). Closed-cell foams are stiffer. The bulk modulus has the same scaling in both cases but different numerical coefficients. Open-cell foams are much softer than closed-cell foams in shear since the modulus scales with $E\phi^2$.

Acknowledgements We thank Jean-Francois Sadoc and Nicolas Rivier for creating a magical experience in Cargese. Sandia is a multiprogram laboratory operated by Sandia Corporation, a Lockheed Martin Company, for the United States Department of Energy under contract #DE-AC04-94AL85000. This work was also supported by the Dow Chemical Company under a Cooperative Research and Development Agreement (CRADA).

References

1. Love, A.E.H. (1994) *A Treatise on the Mathematical Theory of Elasticity*, Dover, New York.
2. Weaire, D. and Fortes, M.A. (1994) Stress and strain in liquid and solid foams, *Advances in Physics*, **43**, 685-738.
3. Kraynik, A.M. (1988) Foam flows, *Ann. Rev. Fluid Mech.*, **20**, 325-357.
4. Gibson, L.J. and Ashby, M.F. (1997) *Cellular Solids: Structure and Properties, 2nd Ed*, Cambridge University Press, Cambridge.
5. Kraynik, A.M. and Warren, W.E. (1994) The elastic behavior of low-density cellular plastics, in N.C. Hilyard and A.C. Cunningham (eds.) *Low Density Cellular Plastics*, Chapman & Hall, London, 187-225.
6. Plateau, J.A.F. (1873) *Statique Experimentale et Theorique des Liquides Soumis aux Seules Forces Moleculaires*. Gauthier-Villiard.
7. Princen, H.M. (1983) Rheology of foams and highly concentrated emulsions. I. Elastic properties and yield stress of a cylindrical model system, *J. Coll. Int. Sci.*, **91**, 160-175.
8. Khan, S.A. and Armstrong, R.C. (1986) Rheology of foams. I. Theory for dry foams, *J. Non-Newtonian Fluid Mech.*, **22**, 1-22.
9. Kraynik, A.M. and Hansen, M.G. (1986) Foam and emulsion rheology: A quasistatic model for large deformations of spatially periodic cells, *J. Rheology*, **30**, 409-439.
10. Reinelt, D.A. and Kraynik, A.M. (1990) On the shearing flow of foams and concentrated emulsions, *J. Fluid Mech.*, **215**, 431-455.
11. Kraynik, A.M., Reinelt, D.A. and Princen, H.M. (1991) The nonlinear elastic behavior of polydisperse hexagonal foams and concentrated emulsions, *J. Rheology*, **35**, 1235-1253.
12. Bolton, F. and Weaire, D. (1991) The effects of Plateau borders in the two-dimensional soap froth. I. Decoration lemma and diffusion theorem, *Philos. Mag. B.*, **63**, 795-809.
13. Bolton, F. and Weaire, D. (1992) The effects of Plateau borders in the two-dimensional soap froth. II. General simulation and analysis of rigidity loss transition, *Philos. Mag. B.*, **65**, 473-487.
14. Hutzler, S., Weaire, D. and Bolton, F. (1995) The effects of Plateau borders in the two-dimensional soap froth. III. Further results, *Philos. Mag. B.*, **71**, 277-289.
15. Warren, W.E. and Kraynik, A.M. (1987) Foam mechanics: The linear elastic response of two-dimensional spatially periodic cellular materials, *Mech. Materials*, **6**, 27-37.
16. Kelvin, Lord (Thompson, W.) (1887) On the division of space with minimum partitional area, *Philos. Mag.*, **24**, 503-514.
17. Weaire, D. and Phelan, R. (1994) A counter-example to Kelvin's conjecture on minimal surfaces, *Phil. Mag. Lett.*, **69**, 107-110.
18. Brakke, K.A. (1992) The surface evolver, *Experimental Mathematics*, **1**, 141-165.
19. Rivier, N. (1994) Kelvin's conjecture on minimal froths and the counter-example of Weaire and Phelan, *Phil. Mag. Lett.*, **69**, 297-303.
20. Nye, J.F. (1985) *Physical Properties of Crystals*, Clarendon Press, Oxford.
21. Matzke, E.B. (1946) The three-dimensional shape of bubbles in foam–an analysis of the role of surface forces in three-dimensional cell shape determination, *Am. J. Botany*, **33**, 58-80.
22. Kraynik, A.M. and Reinelt, D.A. (1996) The linear elastic behavior of dry soap foams, *J. Coll. Int. Sci.*, **181**, 511-520.
23. Kraynik, A.M. and Reinelt, D.A. (1996) The linear elastic behavior of a bidisperse Weaire-Phelan foam, *Chem. Eng. Comm.*, **148-150**, 409-420.
24. Reinelt, D.A. and Kraynik, A.M. (1996) Large elastic deformations of three-dimensional foams and highly concentrated emulsions, *J. Coll. Int. Sci.*, **159**, 460-470.
25. Kraynik, A.M. and Reinelt, D.A. (1996) Elastic-plastic behavior of a Kelvin foam, *Forma*, **11**, 255-270.

26. Reinelt, D.A. and Kraynik, A.M. (1996) Simple shearing flow of a dry Kelvin soap foam, *J. Fluid Mech.*, **311**, 327-343.
27. Kraynik, A.M., and Reinelt, D.A. (1996) The microrheology of wet foams, in A. Ait-Kadi, J.M. Dealy, D.F. James and M.C. Williams (eds.) *Proceedings of XIIth International Congress on Rheology*, Quebec City, Canada, August 18-23, 625-626.
28. Princen, H.M. and Kiss, A.D. (1986) Rheology of foams and highly concentrated emulsions. III. Static shear modulus, *J. Coll. Int. Sci.*, **112**, 427-437.
29. Princen, H.M. (1985) Rheology of foams and highly concentrated emulsions. II. Experimental study of the yield stress and wall effects for concentrated oil-in-water emulsions, *J. Coll. Int. Sci.*, **105**, 150-171.
30. Warren, W.E. and Kraynik, A.M. (1997) Linear elastic behavior of a low-density Kelvin foam with open cells, *ASME J. Appl. Mech.*, to appear.
31. Zhu, H.X., Knott, J.F. and Mills, N.J. (1997) Analysis of the elastic properties of open-cell foams with tetrakaidecahedral cells, *J. Mech. Physics Solids*, **45**, 319-343.
32. Zhu, H.X., Mills, N.J. and Knott, J.F. (1997) Analysis of high strain compression of open-cell foams with tetrakaidecahedral cells, *J. Mech. Physics Solids*, to appear.
33. ABAQUS User's Manual, Version 5.6 (1996) Hibbitt, Karlsson and Sorensen Inc., Providence, Rhode Island.
34. Kusner, R. and Sullivan, J.M. (1996) Comparing the Weaire-Phelan equal-volume foam to Kelvin's foam, *Forma*, **11**, 233-242.
35. Hashin, Z. and Shtrikman, S. (1963) A variational approach to the theory of the elastic behavior of multiphase materials, *J. Mech. Physics Solids*, **11**, 127-140.